AJAE

Open Access

Vol. 13, No. 2, pp. 117-135, June 2019
doi: https://doi.org/10.5572/ajae.2019.13.2.117
ISSN (Online) 2287-1160, ISSN (Print) 1976-6912

Research Article

Meteorological Characteristics and Assessment of the Effect of Local Emissions during High PM_{10} Concentration in the Seoul Metropolitan Area

Il-Soo Park*, Hyeon-Kook Kim[1)], Chang-Keun Song[1)], Yu-Woon Jang[2)], Sang-Heon Kim[3)], Chang-Rae Cho[3)], Jeffrey S. Owen[2)], Cheol-Hee Kim[4)], Kyung-Won Chung[5)], Moon-Soo Park[3),*]

Research Center of Asian Dust and Long-range Transboundary Air Pollutants, Hankuk University of Foreign Studies, Yongin, Republic of Korea
[1)]School of Urban and Environmental Engineering, Ulsan National Institute of Science and Technology, Ulsan, Republic of Korea
[2)]Department of Environmental Science, Hankuk University of Foreign Studies, Yongin, Republic of Korea
[3)]Research Center for Atmospheric Environment, Hankuk University of Foreign Studies, Yongin, Republic of Korea
[4)]Department of Atmospheric Sciences, Pusan National University, Busan, Republic of Korea
[5)]Research Center of Latin America and Caribbean Studies, Hankuk University of Foreign Studies, Seoul, Republic of Korea

***Corresponding author.**
Tel: +82-31-8020-5586
E-mail: moonsoo@hufs.ac.kr
Tel: +82-31-330-4721
E-mail: nierpis@hanmail.net

Received: 29 March 2019
Revised: 25 May 2019
Accepted: 4 June 2019

ABSTRACT In this study, we investigate the meteorological characteristics and the effect of local emissions during high PM_{10} concentrations in the Seoul Metropolitan Area (SMA) by utilizing data from a high-resolution urban meteorological observation system network (UMS-Seoul) and The Air Pollution Model (TAPM). For a detailed analysis, days with PM_{10} concentrations higher than 80 μg m^{-3} for daily average PM_{10} concentration (classified as unhealthy by the Korean Ministry of Environment) in the Seoul Metropolitan Area (SMA) were classified into 3 Cases. Case I was defined as when the prevailing effect was from outside the SMA. Case II was defined as when the prevailing effect was a local effect with outside. Case III was defined as when the prevailing effect was local. Overall, high PM_{10} concentrations in the SMA mostly occurred under weak migratory anticyclone systems over the Korean Peninsula during warm temperatures. Prior to the PM_{10} concentration reaching the peak concentration, the pattern in each case was distinctive. After peak concentrations, however, the pattern for the 3 cases became less distinct. This study showed that nearly 50% of the high PM_{10} concentrations in the SMA occurred in spring and were governed by the conditions for Case II more than these for Cases I and III. In spring, the main sources of the high PM_{10} concentrations in the SMA were local emissions due to the predominance of weak winds and local circulation. The simulation showed that the non-SMA emissions were about 63 to 73% contribution to the spring high PM_{10} concentrations in the SMA. Specifically, local point sources including industrial combustion, electric utility, incineration and cement production facilities scattered around the SMA and could account for PM_{10} concentrations more than 10 μg m^{-3} in the SMA.

KEY WORDS High PM_{10} concentration, Korea, Local emission sources, Local meteorological circulation, Long-range transboundary processes

1. INTRODUCTION

The Seoul metropolitan area (SMA) is a mega city with an area of approximately 11,827 km^2 and a population of 26.1 million inhabitants (http://kosis.kr), and is ranked as the fifth largest urban area population in 2018 (Demographia, 2018). Recently, the number of days with serious concentrations of air pollutants exceeding the national ambient air quality standards of 100 μg m^{-3} (35 μg m^{-3}) for 24-h

PM_{10} ($PM_{2.5}$) concentration has increased (Park *et al.*, 2018; NIER, 2017). For example, the Korean Ministry of Environment (KMOE) issued emergency reduction actions over the SMA on 14 January 2019 when the average $PM_{2.5}$ concentration from 0000 LST (Local Standard Time; UTC + 0900) to 1600 LST was over 50 μg m^{-3} and the forecast average $PM_{2.5}$ concentration for 24 h later was greater than 50 μg m^{-3} (KMOE, 2017). These actions resulted in the prohibition of older diesel vehicles from entering downtown areas in the SMA and a two-shift system for permissible vehicles to enter.

Concerns about air pollution have led to the operation of a modeling system for the daily air quality prediction to support control actions within the SMA (Park *et al.*, 2004). High PM_{10} concentrations in a particular region can be caused by trapped particle emissions and/or local secondary generation of particulate matter through photochemical reactions in the atmosphere (Kim *et al.*, 2017; Seo *et al.*, 2017). Recent high PM_{10} concentrations in Korea appear to partly result from transboundary pollution from China, but also from domestic sources originating from local emissions (Wang *et al.*, 2018; Park *et al.*, 2015, 2005; Jo and Kim, 2013; Kim *et al.*, 2012). From January 1, 2016 to January 31, 2019, there were 65 occurrences of high PM_{10} concentration in the SMA where the daily average PM_{10} concentration without the effect of Asian dust was greater than 80 μg m^{-3} (classified as unhealthy by KMOE). Higher PM_{10} concentrations generally occur on warm days in spring, autumn, or winter and are believed to be closely related to warm temperatures in the atmosphere (Park, 2014). For example, in 2016, an advisory by MOE was in effect over the SMA from April 8 to 12 with a PM_{10} concentration on April 9 of 241 μg m^{-3}.

Previous studies have investigated the occurrence of high PM_{10} concentration in Korea (Park, 2016). During most episodes (Seo *et al.*, 2018), the Korean peninsula is influenced by anticyclonic circulation with warm and humid air with stagnant conditions, based on surface and upper atmosphere maps during high PM_{10} concentration episodes (Seo *et al.*, 2017; Park, 2016). Under these conditions, the stable atmosphere with an inversion layer and thick fog is unfavorable for transport and dispersion of particulate matter (Seo *et al.*, 2018). Other mechanisms for high PM_{10} concentrations, such as transboundary processes from local sources, also need to be considered for a comprehensive understanding of the occurrence of long-lasting high PM_{10} concentration episodes (Park *et al.*, 2018; Park, 2016). Understanding the processes and impacts of both transboundary processes and local emissions is still an important issue for developing effective emission abatement strategies in Korea.

The main objective of this study was to analyze the meteorological characteristics and PM_{10}, $PM_{2.5}$, NO_2, and SO_2 concentrations to assess the effect of local emissions during high PM_{10} concentration. In this study, high PM_{10} concentration in the SMA is defined as when the daily average PM_{10} concentration (without the effect of Asian dust) is greater than 80 μg m^{-3}. All results representing the SMA refer to central Seoul, the capital city of South Korea.

2. MATERIALS

2.1 Meteorological and Air Quality Data

Hourly mean air quality data such as PM_{10}, $PM_{2.5}$, SO_2, NO_2, and O_3 concentrations at Seoul and Baengnyeongdo (BND) stations were used (http://www.airkorea.or.kr) (Fig. 1). Seoul station is located near the City Hall and at the center of Seoul, and is surrounded by many line and area sources (cross mark in Seoul in Fig. 1). The BND station, one of national background air quality monitoring station, has few nearby anthropogenic emission sources (cross mark in BN in Fig. 1). It is located about 208 km west of Seoul Station (Fig. 1). Surface meteorology and boundary structure were obtained from the surface energy balance observation tower and the lidar-type ceilometer installed at Jungnang Station (diamond in Seoul in Fig. 1; Park, 2018; Park *et al.*, 2017). The station is located 9 km east of Seoul Station. Temperature, relative humidity, wind speed and direction, downward solar radiation, and 3-dimensional sonic anemometer sensors are installed on a surface energy balance tower. Friction velocity is computed by applying an eddy covariance method using 30-min block averaging with 10-Hz meridional, zonal, and vertical wind speed (Kwon *et al.*, 2014; Park *et al.*, 2014). A ceilometer (model: CL51, manufacturer: Vaisala) gives vertical profiles (10-m vertical resolution) of two-way attenuated backscatter due to atmospheric aerosols by means of 910 nm wavelength laser. Backscatter exceeding 400×10^{-8} sr^{-1} m^{-1} was excluded to remove the effects of high backscatter media such as clouds (Park, 2018).

2.2 High PM_{10} Concentrations Classification

When daily mean PM_{10} concentration in Seoul was

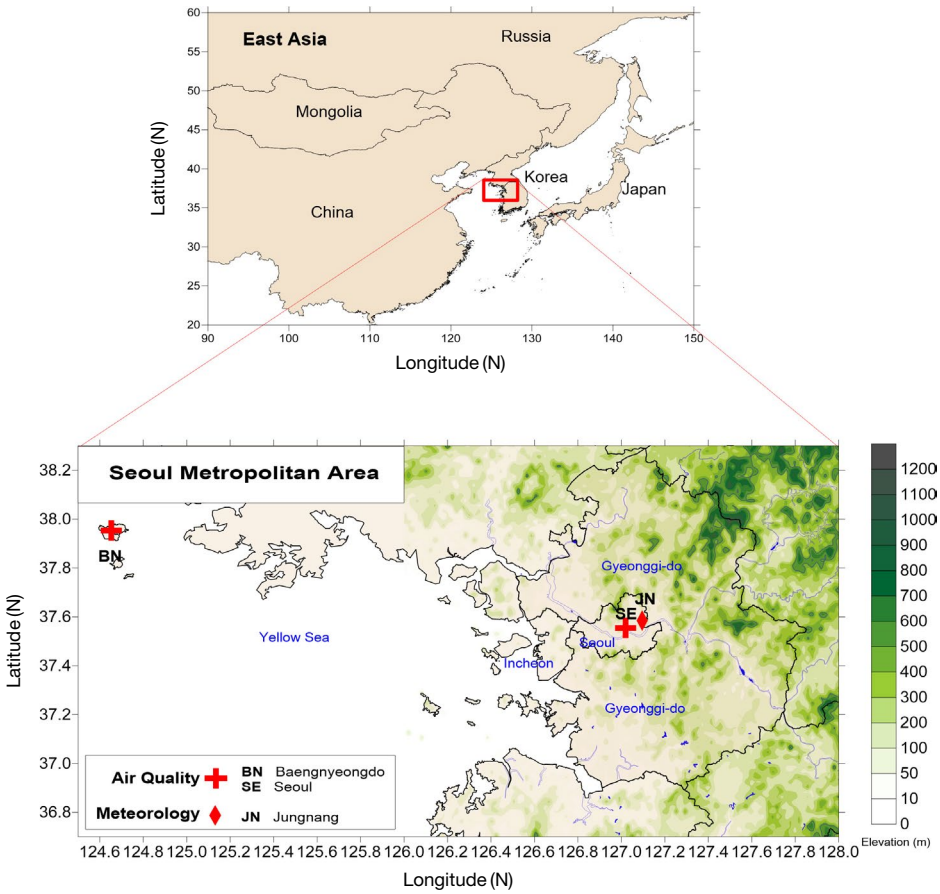

Fig. 1. Location of air quality monitoring and meteorological stations in the study area.

higher than 80 μg m^{-3}, the day was classified as a high PM_{10} concentration. As shown in Table 1, there were 65 high PM_{10} concentration days in the SMA during the period from January 1, 2016 to January 31, 2019. In order to compare the characteristics of high PM concentration, the high PM concentrations days were categorized into 3 Cases: Case I was defined as when the PM_{10} concentration in BND area was higher than that in the SMA, and the PM_{10} ($PM_{2.5}$) concentration at BND Station was higher than 100 μg m^{-3} (50 μg m^{-3}). The high PM_{10} in this case could be considered to be transported from mainly long-range transboundary processes; Case II was defined as when the PM_{10} concentration in BND was lower than that in the SMA, and the PM_{10} ($PM_{2.5}$) concentration was higher than an annual mean of 38 μg m^{-3} (22 μg m^{-3}) at BND. As mentioned, because the BND station is far from direct emission sources, the mean PM concentration in BND was much lower than that in Seoul. Thus, annual mean concentrations at BND were considered to discriminate local-emission from contributions from long-range transboundary processes. High PM concentrations in this case could be result from both local and long-range transboundary processes; Case III was defined as when the PM_{10} ($PM_{2.5}$) concentration at BND was lower than 38 (22) μg m^{-3}, or the $PM_{2.5}$ concentration at BND was lower than one-half of that in the SMA. High PM concentrations in this case could be considered to be emitted from mainly local sources. Annual mean PM concentrations at BND rather than the national standards would be enough to reveal

Table 1. Number of high PM_{10} and $PM_{2.5}$ occurrence days for the 3 cases among 65 occurrences of high PM_{10} concentration (over 80 μg m^{-3} in the SMA, $PM_{2.5}$ in parenthesis).

Season	Case I	Case II	Case III	Total
Spring	4 (8)	26 (19)	2 (5)	32 (32)
Autumn	–	2 (2)	2 (–)	4 (2)
Winter	8 (13)	17 (13)	4 (3)	29 (29)

Monitoring data for $PM_{2.5}$ was missing for 2 days.

Table 2. Daily average PM_{10}, $PM_{2.5}$, NO_2, SO_2, CO, and O_3 concentrations for the 3 cases of high PM_{10} concentrations selected in this study.

Case	Season (Date)	PM_{10} ($\mu g\ m^{-3}$)	$PM_{2.5}$ ($\mu g\ m^{-3}$)	NO_2 (ppb)	SO_2 (ppb)	CO (ppm)	O_3 (ppb)
Case I	Spring (April 30, 2017)	91[1)] 157[2)]	49[1)] 57[2)]	22[1)] 6[2)]	8[1)] 4[2)]	0.6[1)] 0.3[2)]	71[1)] 71[2)]
	Winter_a (January 20, 2018)	102 160	63 108	47 10	7 5	0.9 1.4	13 34
	Winter_b (January 13, 2019)	115 122	83 97	49 6	6 3	1.1 0.9	13 49
Case II	Spring (March 12, 2018)	99[1)] 46[2)]	64[1)] 33[2)]	55[1)] 6[2)]	6[1)] 2[2)]	0.8[1)] 0.2[2)]	19[1)] 57[2)]
	Autumn (November 18, 2016)	94 81	54 49	56 20	6 3	1.0 0.5	5 27
	Winter (December 22, 2018)	88 51	63 37	54 5	7 1	1.0 0.5	9 33
Case III	Spring (March 26, 2018)	106[1)] 19[2)]	71[1)] 13[2)]	50[1)] 5[2)]	6[1)] 2[2)]	0.8[1)] 0.5[2)]	25[1)] 63[2)]
	Autumn (November 6, 2018)	102 30	71 20	63 4	5 2	1.0 0.7	5 35
	Winter (February 4, 2017)	96 38	70 31	61 10	5 3	1.1 0.3	4 33

[1)]Daily average concentration in the SMA. [2)]Daily average concentration in BND.

contrasts between local-emission and long-range transboundary processes in the SMA.

According to the above criteria, around 70% (45) of all high PM_{10} concentration days was classified as Case II, while 18% (12) and 12% (8) were Case III and I, respectively (Table 1). Also, 49% and 45% were occurred in spring and winter, respectively, while only 6% was occurred in autumn. For investigation of detailed features, 3 events for all cases were selected: one spring and two winter (no event in autumn) were selected for Case I. One event in each season (spring, autumn, and winter) for Case II and III was selected, respectively. Table 2 shows the daily mean PM_{10}, $PM_{2.5}$, NO_2, SO_2, CO, and O_3 concentrations at BND and Seoul Stations for all high PM_{10} concentration days.

3. CHARACTERISTICS OF AIR POLLUTANTS

Time series of PM_{10}, $PM_{2.5}$, NO_2, and SO_2 concentration during the 7 days centered on the high concentration day at SMA and BND are shown in Fig. 2. Median concentrations and ratios of the 7-day mean concentration to the monthly mean concentration for each case and each pollutant are summarized in Tables 3 and 4, respectively. The detailed features of the temporal variation were analyzed for each case.

Case I: The PM_{10} and $PM_{2.5}$ concentrations in Seoul showed a lag time 6 to12 h for the maximum concentration compared to those in BND during high PM_{10} concentration for all cases. The maximum PM_{10} concentration of 111 $\mu g\ m^{-3}$ (180 $\mu g\ m^{-3}$) in Seoul was much lower than 386 $\mu g\ m^{-3}$ (299 $\mu g\ m^{-3}$) at BND for the spring (winter_a) case (Fig. 2). Because there were few direct NO_2 sources at BND, NO_2 concentrations at BND were much lower than in the SMA during the study period. The SMA had nearly the same SO_2 or lower concentration than BND. The median values in the SMA were nearly the same as in BND for PM_{10}, $PM_{2.5}$, and SO_2 concentrations, while much higher than BND for NO_2 concentration (Fig. 3; Table 3). The ratio of the 7-day mean concentration to monthly mean concentration showed high values for PM_{10} and $PM_{2.5}$ concentration, while nearly the same values for NO_2 and SO_2 at both the SMA and BND (Table 4).

Case II: The PM_{10} and $PM_{2.5}$ concentrations in the SMA were nearly the same as concentrations in BND. NO_2 concentration in BND was much less than that in the SMA, while SO_2 concentration in the SMA was higher than that in BND, especially in winter (Fig. 2). In autumn, high PM_{10} concentrations in BND were observed later than in the SMA by about 6 h, and high NO_2 concentration in BND were recorded on 18–19 November 2016. These implied that air parcels in BND might be

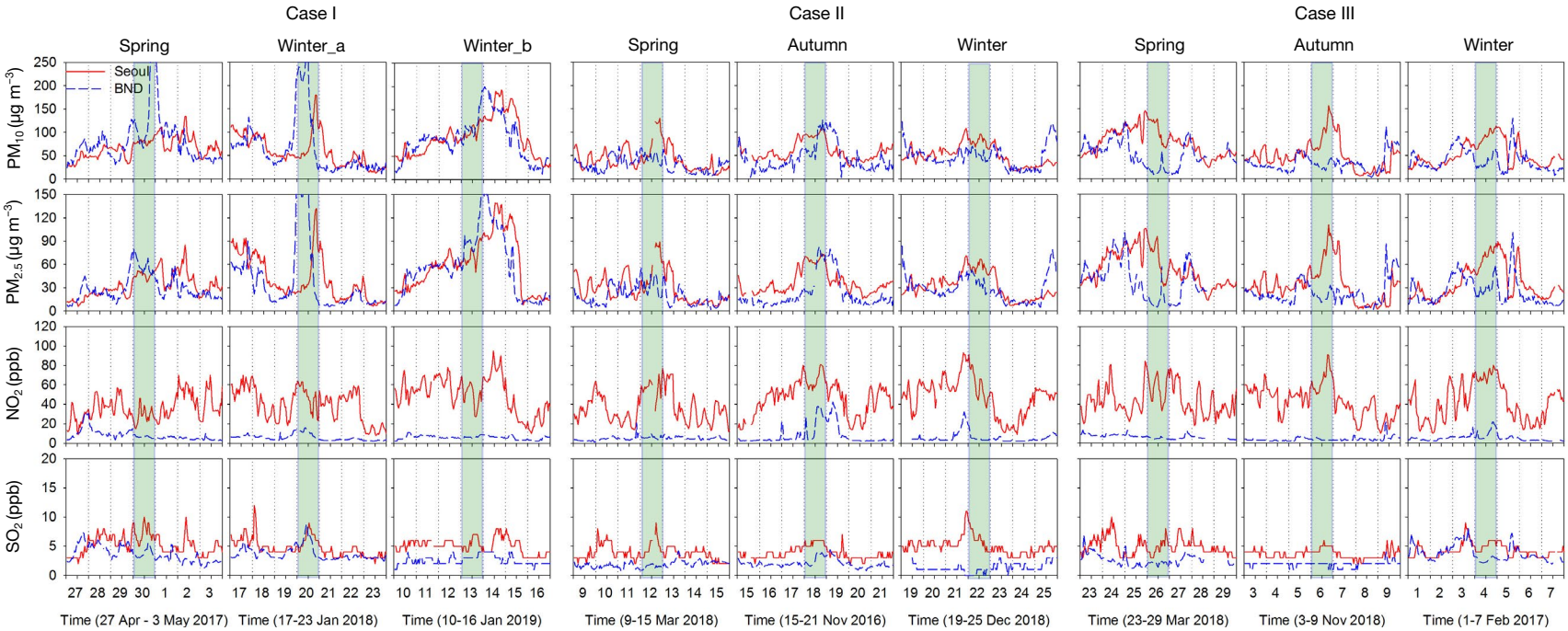

Fig. 2. Time series of PM_{10} (first panel), $PM_{2.5}$ (second panel), NO_2 (third panel), and SO_2 (fourth panel) concentrations in the SMA and BND during the 7 consecutive days around the maximum concentration for each case. High PM_{10} concentration days are shown by green shading.

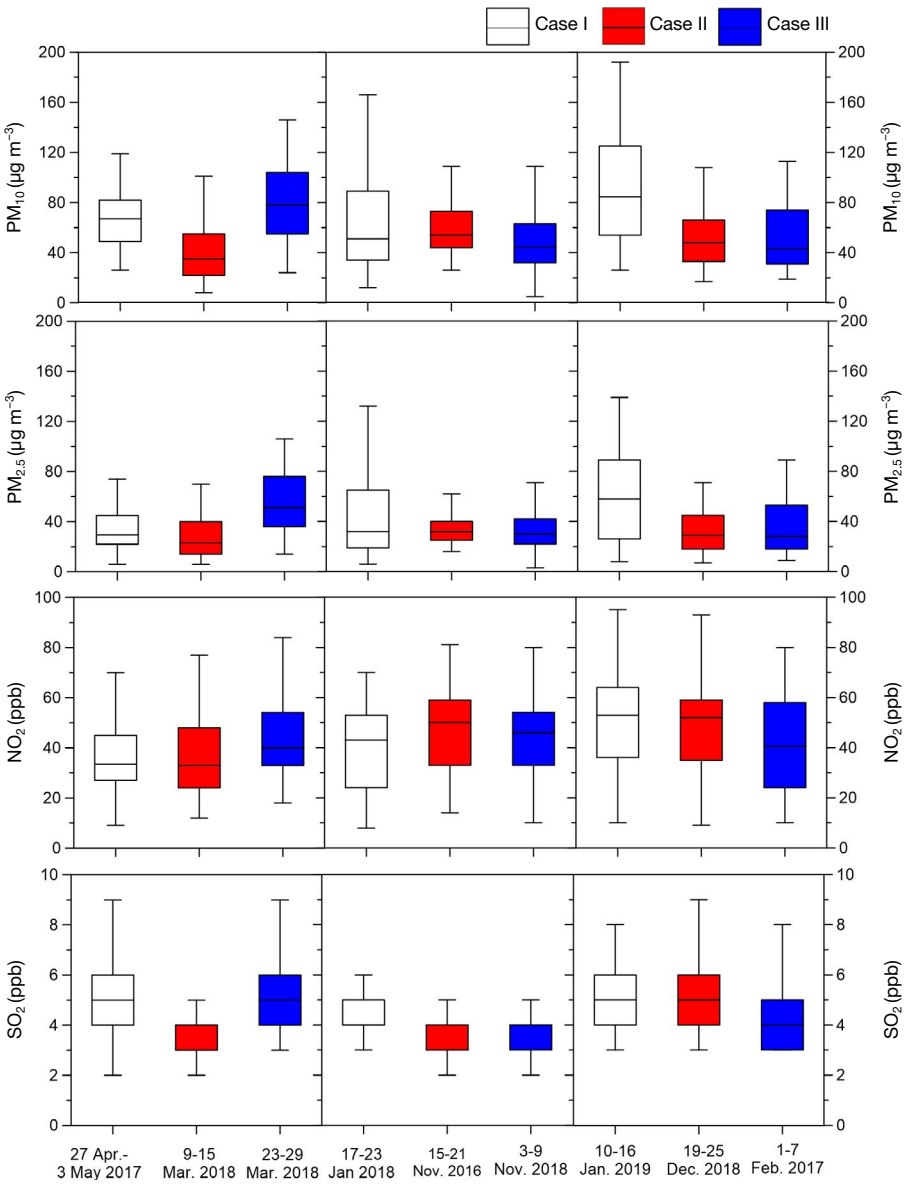

Fig. 3. Boxplots of PM_{10} (first panel), $PM_{2.5}$ (second panel), NO_2 (third panel), and SO_2 (fourth panel) concentrations in the SMA during the 7 consecutive days around the maximum concentration for each case.

advected from the SMA. The median values in the SMA were similar to or higher than BND for PM_{10}, $PM_{2.5}$, and SO_2 concentrations, while much higher than BND for NO_2 concentration (Table 3). The ratios of the 7-day mean concentration to the monthly mean concentration were more or less unity except for high for PM concentrations in both areas in winter and low SO_2 concentrations at BND in autumn and winter (Table 4).

Case III: The PM_{10} and $PM_{2.5}$ concentrations in the SMA were nearly the same as concentrations at BND prior to the high PM concentration period in the SMA. However, PM concentrations in the SMA increased, but those in BND sharply decreased (Fig. 2). These implied that prior to the peak of PM concentration in the SMA, the SMA might be influenced by air masses that passed the BND region. But after the peak, SMA and BND might be influenced by different air masses. So high PM concentration in the SMA was mainly contributed by local emission. The NO_2 and SO_2 concentrations in BND were much less than concentrations in the SMA, except for SO_2 concentrations in winter. The median concentrations in the SMA were much higher than those

Table 3. Median PM_{10}, $PM_{2.5}$, NO_2, and SO_2 concentrations in the SMA and BND for the 3 cases.

Case	Season	Season (Date)	PM_{10} ($\mu g\ m^{-3}$)	$PM_{2.5}$ ($\mu g\ m^{-3}$)	NO_2 (ppm)	SO_2 (ppm)
I	Spring	Apr 27–May 3, 2017	67.0[1)] 68.0[2)]	29.5[1)] 24.0[2)]	0.034[1)] 0.006[2)]	0.005[1)] 0.003[2)]
	Winter_a	Jan 17–23, 2018	51.0 39.0	32.0 19.0	0.043 0.004	0.004 0.003
	Winter_b	Jan 10–16, 2019	84.5 86.0	58.0 55.0	0.053 0.006	0.005 0.002
II	Spring	Mar 9–15, 2018	35.0[1)] 30.0[2)]	23.0[1)] 17.0[2)]	0.033[1)] 0.004[2)]	0.004[1)] 0.002[2)]
	Autumn	Nov 15–21, 2016	54.0 34.0	32.0 14.0	0.050 0.003	0.003 0.002
	Winter	Dec 19–25, 2018	48.0 45.5	29.0 27.0	0.052 0.004	0.005 0.001
III	Spring	Mar 23–29, 2018	78.0[1)] 51.0[2)]	51.0[1)] 38.0[2)]	0.040[1)] 0.007[2)]	0.005[1)] 0.002[2)]
	Autumn	Nov 3–9, 2018	44.5 28.5	30.0 19.0	0.046 0.003	0.004 0.002
	Winter	Feb 1-7, 2017	43.0 32.0	28.0 19.0	0.041 0.005	0.004 0.003

[1)]SMA, [2)]BND

Table 4. Ratio of the 7-day average concentration (calculated as three days before and three days after the maximum concentration) to the monthly average concentration for the 3 cases.

	Spring			Autumn		Winter			
	Case I	Case II	Case III	Case II	Case III	Case I (a)	Case I (b)	Case II	Case III
PM_{10}	1.24[1)] 1.33[2)]	0.94 0.80	1.76 1.35	1.17 0.86	1.02 0.84	1.33 1.53	1.53 1.61	1.21 1.37	1.18 1.07
$PM_{2.5}$	1.22[1)] 1.10[2)]	0.98 0.85	1.84 1.70	1.15 0.82	1.23 1.23	1.36 1.67	1.78 1.99	1.29 1.52	1.29 1.19
NO_2	0.95[1)] 1.28[2)]	1.06 0.96	1.26 1.34	1.16 1.50	1.09 1.10	1.15 1.23	1.19 1.15	1.35 1.46	1.09 1.13
SO_2	1.30[1)] 1.34[2)]	1.02 0.89	1.31 1.24	1.03 0.77	0.99 1.02	1.06 1.18	1.10 0.95	1.29 0.60	1.00 1.02

[1)]SMA, [2)]BND

in BND for PM_{10}, $PM_{2.5}$, and NO_2 (Fig. 3; Table 3). The ratios of the 7-day mean concentration to the monthly mean concentration were larger than unity in spring, but more or less unity in autumn, and winter (Table 4).

4. METEOROLOGICAL CHARACTERISTICS

4.1 Synoptic Analyses

To identify the impacts of meteorological conditions on PM concentrations, surface weather charts near the Korean Peninsula at 0900 LST for selected event days shown in Fig. 4 were investigated.

Case I: A relatively small-scale high pressure system affected the entire Korean Peninsula for all event days. It started from northwest of the Korean Peninsula, and was separated from the periphery of the Siberian High, especially in winter (Fig. 4b, c). A small anticyclonic system, originated from rear-side of the upper trough, passed through the Korean peninsula from northwest to southeast in spring (Fig. 4a).

Case II: A weak anticyclone system, separated from the high pressure system centered on the Japanese Islands, was stagnant over the Korean Peninsula in spring and autumn (Fig. 4d, e). The SMA was affected by a small-scale high pressure system originating from the Siberian High in winter (Fig. 4f). Due to the position of

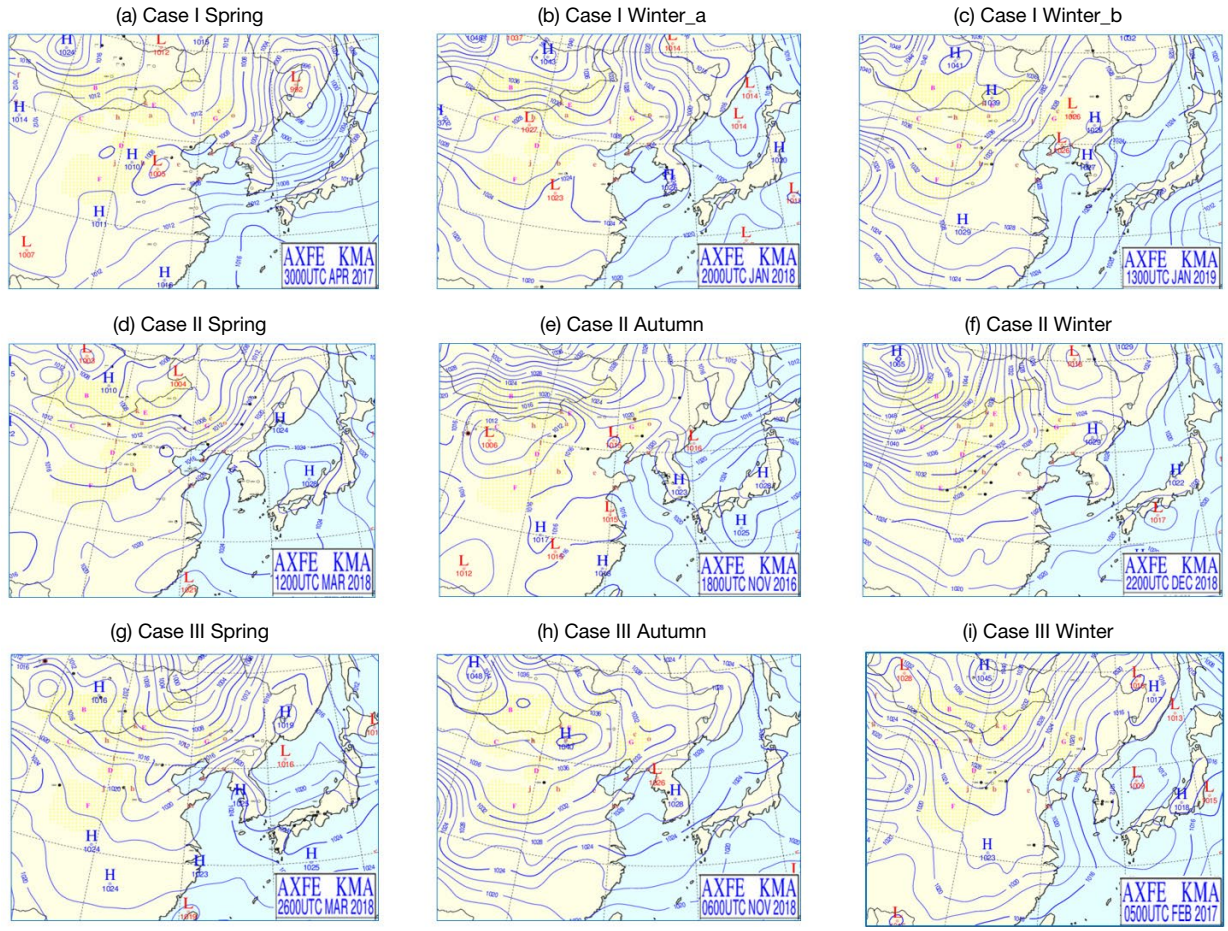

Fig. 4. Surface weather charts near the Korean peninsula at 0900 LST on (a) 30 April 2017, (b) 20 Jan 2018, (c) 13 Jan 2019, (d) 12 Mar 2018, (e) 18 Nov 2016, (f) 22 Dec 2018, (g) 26 Mar 2018, (h) 06 Nov 2018, and (i) 05 Feb 2017 for high PM_{10} concentration days.

the weak high pressure system near the Korean Peninsula in autumn and winter, weak easterly winds became dominant in the SMA. The easterly wind might be evidence for advection from SMA to BND in autumn and winter, and the high NO_2 concentration in BND (Fig. 2).

Case III: The synoptic meteorological patterns in spring and winter were similar to that for the Case II autumn case (Fig. 4g, h). A small-scale high pressure system, separated from the southern part of the Korean Peninsula, was stationary over the SMA in winter (Fig. 4i).

Overall, most high PM concentration episodes in the SMA were accompanied by weak migratory anticyclone systems over the Korean Peninsula. The horizontal extent of surface pressure near the Korean Peninsula for all cases were very small, implying that the synoptic system near the SMA was weak and stagnant during the event periods, as previous studies have shown (Park, 2018; Seo *et al.*, 2017).

4.2 Surface Meteorology and Boundary-Layer Structure

In order to understand the effect of surface meteorology and boundary-layer structure on PM_{10} and $PM_{2.5}$ concentrations near the surface, time series of meteorological variables (Fig. 5) and the time-height cross section of attenuated backscatter (Fig. 6) measured at Jungnang Station were analyzed (Fig. 1).

Case I: Strong south-westerlies were dominant for the spring case, but weak winds with local circulation were dominant for the winter case (Fig. 5). Air temperature showed an increasing trend for the spring case, and had nearly the same trend but was much warmer than the climatological mean (−2.8 to −2.2°C) for the winter case (http://www.kma.go.kr). Solar radiation during the high PM_{10} episode was lower than on the antecedent clear days. It was due to high scatter of incident solar radiation by atmospheric aerosol (Barmpadimos *et al.*, 2011). A

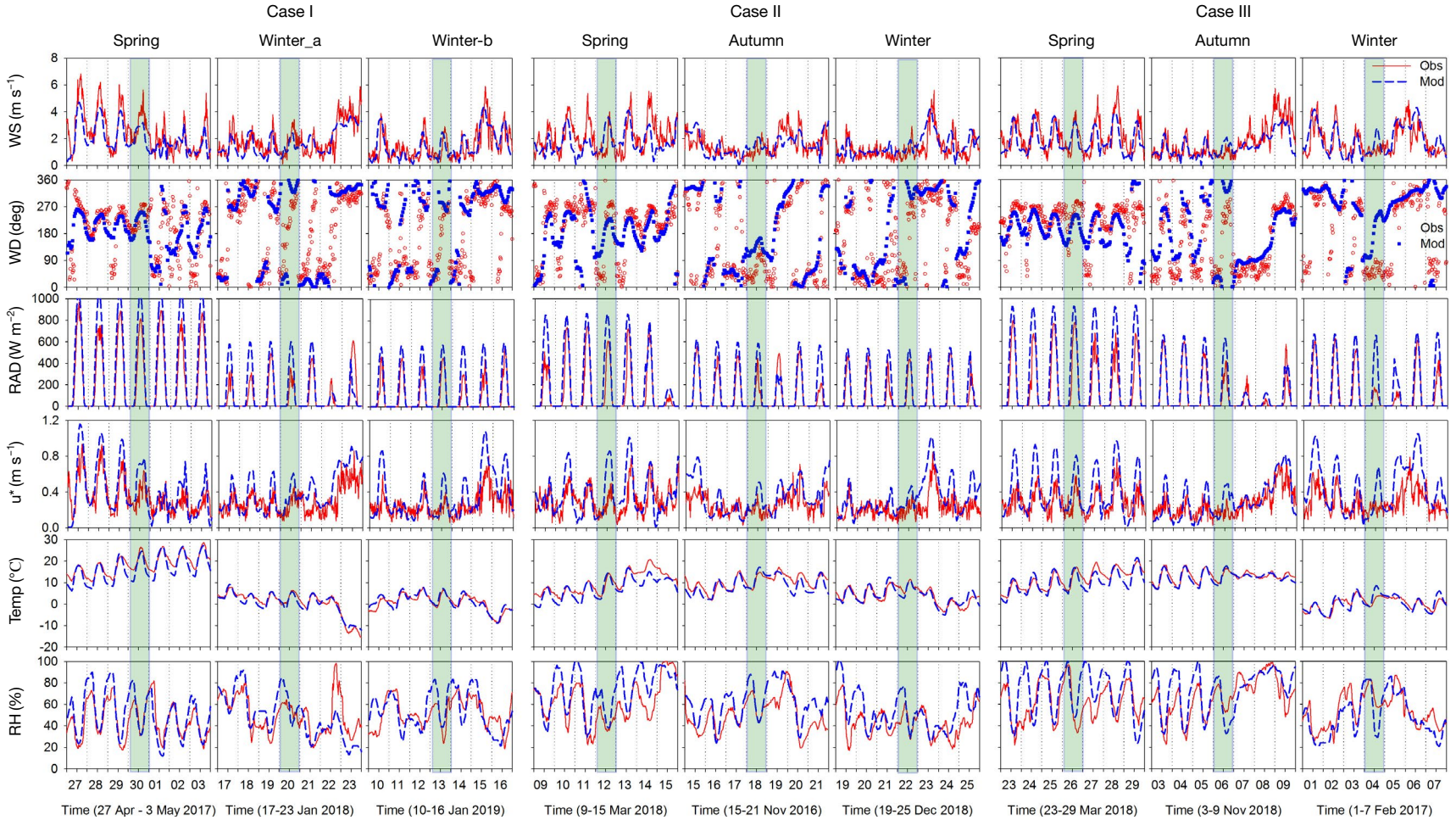

Fig. 5. Time series of observed (red line and open circle) and simulated (blue dashed line and closed rectangle) wind speed (first row), wind direction (second row), net solar radiation (third row), friction velocity (fourth row), air temperature (fifth row), and relative humidity (sixth row) at Jungnang station during the 7 consecutive days around the maximum concentration for each case. High PM_{10} concentration days are shown by green shading.

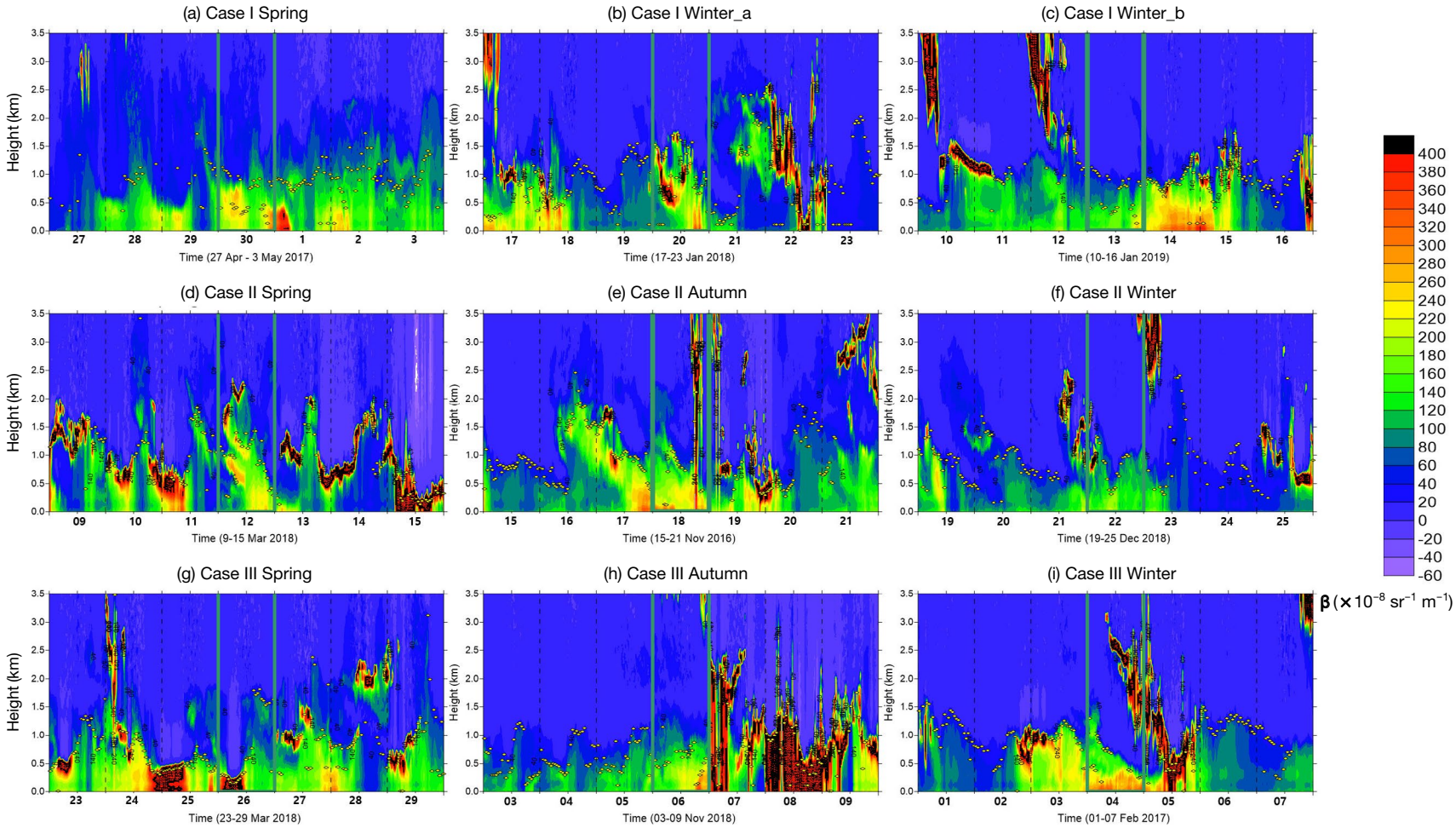

Fig. 6. Time-height cross section of attenuated backscatter and time series of mixing layer height at Jungnang station during the 7 consecutive days around the maximum concentration for each case (a-i).

precipitation event of 3.3 mm was recorded on January 22, 2018. The friction velocity indicated mechanical turbulence and was proportional to wind speed. Weak friction velocity meant the poor vertical and horizontal diffusion (Li *et al.*, 2018). Attenuated backscatter near the surface tended to be proportional to the PM_{10} concentration (Fig. 2). The aerosol layer formed at 300–700 m in the morning, and descended to the surface in the evening on April 30, 2017 in spring. For the winter_a case, an aerosol layer formed near about 1 km height at 0000 LST, and intruded into the lower height (600 m) at 0600 LST on January 20, 2018. The aerosol layer combined with the evolving mixing layer in the morning, and exhibited the maximum PM_{10} concentration near surface in the early evening. For the winter_b case, the aerosol layer formed near the surface and in the overlying residual layer, respectively, at 0000 LST on January 11, 2019. The upper aerosol intruded into the evolving mixing layer two times: from 1 km height in the morning on January 12, and from 500 m height at 0300 LST on January 13, 2019. As a result, the maximum PM_{10} concentration at the surface occurred during the late evening on January 14, 2019.

Case II: Relatively strong westerlies were dominant for the spring case like Case I, but very weak north-easterly winds accompanied by local circulation were dominant for the autumn and winter cases (Fig. 5). The air temperature was much warmer than the climatology (3.9 to 5.9°C for the spring case; 5.6 to 7.0°C for the autumn case; −0.18 to 0.4°C for the winter case). Solar radiation on the high PM_{10} concentration day was lower than on antecedent clear days. Weak northeasterly wind occurred in the morning and the aerosol layer at 1 km height intruded into the mixing layer in the afternoon on March 12, 2018 for the spring case (Park and Chae, 2018). For the autumn case, the aerosol layer at 1.5 km height on November 16, 2016 intruded into the mixing layer in the next afternoon (Fig. 6). After a weak rain in the late evening, PM_{10} concentrations decreased on the next day. For the winter case, a weak aerosol layer intruded into the surface layer on December 20, 2018 and in the morning on December 22, 2018, respectively.

Case III: Relatively strong westerlies were dominant for the spring and winter cases, but weak northeasterly winds were dominant for the autumn case. Differing PM_{10} concentrations in the SMA and BND was accompanied by southwesterly winds for the spring case, and northeasterly winds for the autumn and winter cases (Fig. 5). Air temperature showed an increasing trend for the spring case, and was warmer than the climatology (9.3 to 10.4°C for the autumn case, and −2.4 to −0.9°C for the winter case). The aerosol layer was trapped in the lowest 500 m and 300 m in the morning on 25 and 26 March 2018 for the spring case, respectively. There was no intrusion from the upper layer for the autumn case (Fig. 6). After the high PM_{10} concentration, a heavy rain event (64 mm) occurred on the next day. The aerosol layer was trapped in the lower 300 m under weak wind and a weak aerosol layer intruded from 1 km height on February 4, 2017 for the winter case.

5. TAPM MODELING

TAPM employed in this study is composed of two prognostic subsections: meteorological and chemical modules (Hurley, 2008). The TAPM meteorological module predicts gridded three-dimensional meteorology and air pollutant concentrations. The meteorological component of TAPM is an incompressible, non-hydrostatic, primitive equation model with a terrain-following vertical coordinate for three-dimensional simulations. The model solves the primitive meteorological equations: momentum, temperature, water vapor specific humidity, and cloud/rain/snow components. It includes parameterizations for cloud/rain/snow micro-physical processes, turbulence closure, urban/vegetation canopy and soil, and radiative fluxes (Hurley, 2008). The chemical component of TAPM consists of an Eulerian grid-based set of prognostic equations for both gas and particulate components. TAPM includes gas phase photochemical reactions based on semi-empirical mechanisms called the generic reaction set (GRS) of Azzi *et al.* (1992) with the hydrogen peroxide modification of Venkatram *et al.* (1997). More details on TAPM equations and descriptions can be found in Hurley (2008) and Hurley *et al.* (2008).

The domain for TAPM in this study was based on grids of 100 × 100 × 25 at three domains (12 km, 4 km, 2 km), centered in central Seoul (latitude 37°33.970′N and longitude 126°58.671′E). The initial conditions of the meteorological variables, LAPS (Local Administrator Password Solution) data with a resolution of 75 km × 100 km (ftp://ftp.csiro.au/TAPM) and surface and land use data (1 km × 1 km) from the USGS (United States Geological Survey) (Hurley, 2008) were used.

Table 5. Initial background concentrations for TAPM modeling in this study.

Case	Season	PM_{10} ($\mu g\ m^{-3}$)	$PM_{2.5}$ ($\mu g\ m^{-3}$)	NO_2 (ppb)	SO_2 (ppb)	CO (ppm)	O_3 (ppb)
Case I	Spring	60.3	23.6	21.4	5.2	0.5	43.6
	Winter_a	76.7	52.5	33.8	4.9	0.7	16.2
	Winter_b	71.9	47.5	31.3	3.8	0.8	21.1
Case II	Spring	54.6	37.8	23.1	4.1	0.6	29.3
	Autumn	65.4	32.3	31.5	4.9	0.6	15.2
	Winter	54.0	34.6	34.6	3.5	0.7	18.4
Case III	Spring	85.1	62.1	26.9	4.9	0.6	39.7
	Autumn	40.4	28.1	26.0	2.8	0.7	33.6
	Winter	43.1	25.1	28.1	5.1	0.6	21.6

Nationwide average concentrations of PM_{10}, $PM_{2.5}$, SO_2, NO_2, CO, and O_3 during 3 days before the maximum PM_{10} concentration were used for the initial background model conditions (Table 5). A spin-up time of 5 days was applied to minimize the initial condition influences for both surface and non-surface concentrations.

5.1 Emissions

Total and categorized (area, line, point) emissions of PM_{10}, NO_x, SO_2, and CO in nationwide and in the SMA for 2015 were used in this study. Total emissions were 232,794 ton y^{-1}, 1,000,064 ton y^{-1}, 351,010 ton y^{-1}, and 941,238 ton y^{-1} nationwide and 44,385 ton y^{-1}, 289,431 ton y^{-1}, 37,223 ton y^{-1}, and 307,929 ton y^{-1} in the SMA for PM_{10}, NO_x, SO_2 and CO, respectively (Table 6). PM_{10} and CO emissions mostly originate from area sources, while most of the NO_x emissions are from line sources and SO_2 emissions are from point sources (Park *et al.*, 2004). Each of these source categories were considered and urban-scale air pollutants were accurately inventoried by taking into account of all the information on stationary sources such as stack height, stack diameter, exit velocity, and temperature. Fig. 7 illustrates the spatial distribution of total and apportioned categorized emissions for PM_{10}, NO_x, and SO_2 for each grid (in ton y^{-1} (2 km × 2 km)$^{-1}$). Total emissions of PM_{10} and NO_x were found to be highly dependent on traffic densities, and the largest emission occurred in the central SMA, along expressways, and at junctions of major roads or streets. High emissions of SO_2 were found along the western coastal area, where higher densities of power plants and industries are located (Park *et al.*, 2004).

Table 6. Nationwide and SMA emission of PM_{10}, NO_x, SO_2, and CO (year 2015). (unit: ton y^{-1})

		PM_{10}	NO_x	SO_2	CO
Nationwide	Area	162,777	314,884	111,146	556,560
	Line	55,193	311,957	186	264,919
	Point	14,825	373,223	239,678	119,759
	Total	232,794	1,000,064	351,010	941,238
SMA	Area	27,470	95,888	16,164	144,618
	Line	14,967	119,904	77	111,015
	Point	1,948	73,639	20,982	52,296
	Total	44,385	289,431	37,223	307,929

Table 7. Mean bias (MB), root mean square error (RMSE), correlation coefficient (R), and index of agreement (IOA) between simulated and observed meteorological variables and PM_{10} concentration for Case 1 spring, Case 2 autumn, and Case 3 winter.

Case		Temperature	Wind speed	Wind direction	PM_{10}
Case I Spring	MB	−2.21	−0.59	−12.67	38.36
	RMSE	3.08	1.05	76.4	62.9
	R	0.94	0.82	0.50	0.02
	IOA	0.93	0.77	0.60	0.61
Case II Autumn	MB	−1.37	0.02	48.7	24.5
	RMSE	2.76	0.78	134.7	50.6
	R	0.81	0.48	0.47	0.15
	IOA	0.89	0.71	0.71	0.68
Case III Winter	MB	0.10	0.09	74.3	9.48
	RMSE	1.94	0.88	130.4	44.4
	R	0.85	0.69	0.51	0.40
	IOA	0.93	0.85	0.60	0.77

5.2 Model Evaluation

In order to validate the simulated results, the simulated PM_{10} concentrations at Seoul station and simulated meteorology at Jungnang station, located 11 km from central Seoul were used. The evaluations were performed by using statistical performance measures such

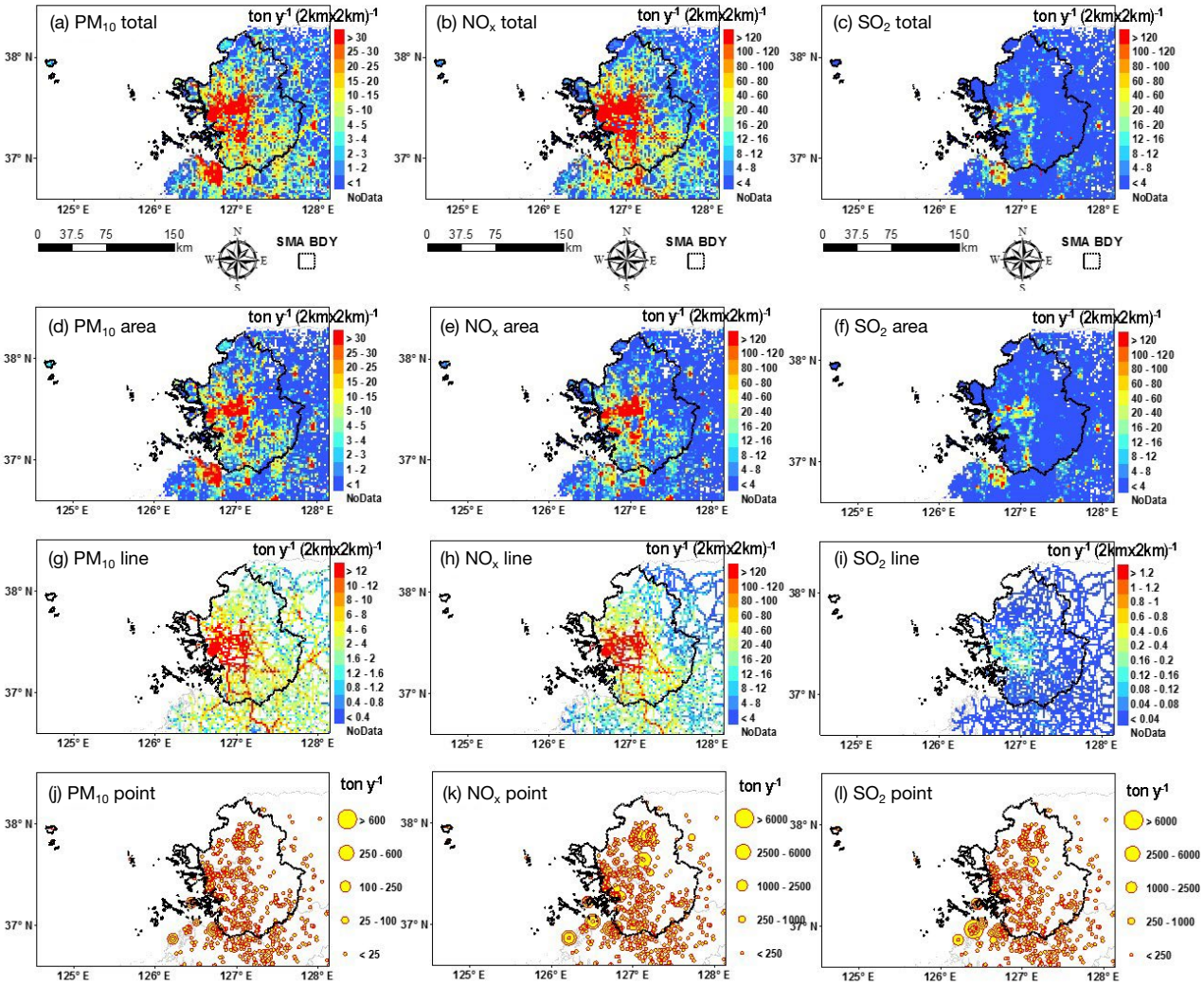

Fig. 7. Spatial distribution of air pollutant emissions in the SMA. Total emissions for PM_{10} (a), NO_x (b) and SO_2 (c); area source emissions for PM_{10} (d), NO_x (e) and SO_2 (f); line source emissions for PM_{10} (g), NO_x (h) and SO_2 (i); point source emissions for PM_{10} (j), NO_x (k) and SO_2 (l). Black-dotted line represents the boundary of SMA.

as the index of agreement (IOA), root mean square error (RMSE), and correlation coefficient (R). IOA is a frequently used measure of how well the predicted variation about the observed mean is represented, with a value greater than about 0.50 considered to indicate a good prediction (Hurley *et al.*, 2008).

Simulated meteorological variables were, by and large, well coincident with the observed ones for all cases (Fig. 5). Wind speed was slightly underestimated under strong wind, while downward solar radiation was overestimated by around 10% in spring. Nighttime temperature (relative humidity) were underestimated (overestimated) in spring. These differences were mainly due to the urban heat island (Park and Chae, 2018). TAPM exhibited some weaknesses in simulating the urban heat island over vast urban surfaces. In order to verify the performance of the model, the mean bias (MB), root mean square error (RMSE), correlation coefficient (R), and index of agreement (IOA) for Case I Spring, Case 2 Autumn, and Case 3 Winter cases were evaluated (Table 7). The results showed that the meteorology (temperature, wind speed, and wind direction) were reasonably well simulated for all selected cases. For PM_{10} concentration, the IOAs were above 0.6, indicating the simulated PM_{10} concentration was in good agreement with observed concentration (Hurley *et al.*, 2008). The IOAs in this

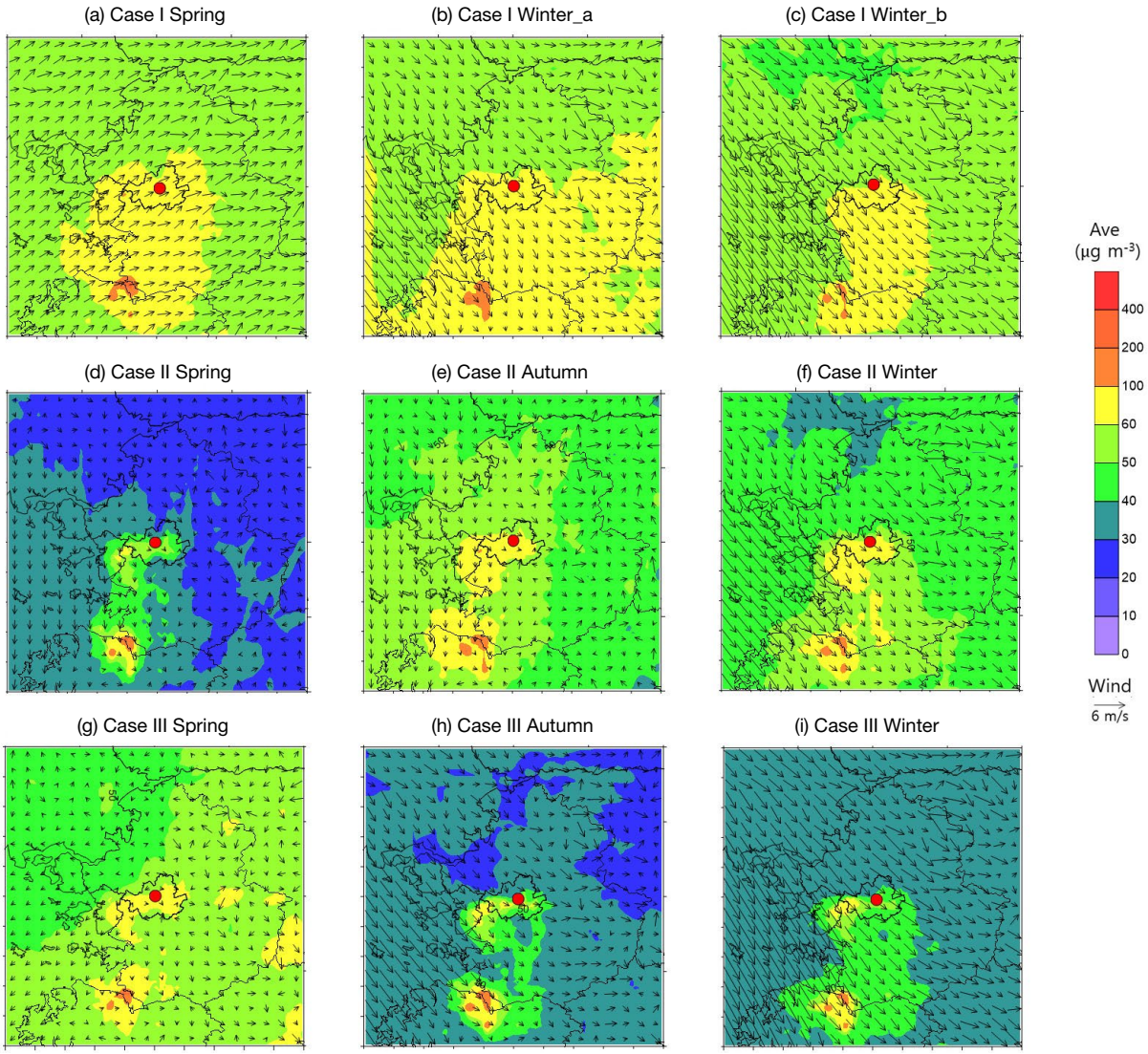

Fig. 8. Horizontal distribution of predicted wind and PM_{10} concentration with the use of nationwide emission in the SMA for each case (a-i). Domain size is 100 km × 100 km with a center at Seoul Station indicated by a red solid circle.

study were found to be generally better than those in recent similar studies in urban areas (Park *et al.*, 2018).

5. 3 Wind and Concentration Fields

Fig. 8 shows the horizontal distribution of PM_{10} with the wind vector simulated with nationwide emissions for the 3 cases. The patterns are strongly governed by the wind; upwind regions had lower concentrations while downwind regions had higher concentrations. The areas where confluence of wind occurred had higher concentrations and areas where the wind diverged had lower concentrations. The overall concentration field in spring and autumn showed an inhomogeneous horizontal distribution pattern. The highest concentration was in the western coastal area due to the high density of point sources such as power plants, industrial complexes and steel production facilities, and also high in the central SMA due to the high density of line sources, with somewhat higher PM_{10} concentrations in the southeast due to the presence of cement manufacturing facilities. The PM_{10} concentration in winter was higher in the southern area due to the prevailing northwesterly wind and showed a more homogeneous horizontal distribution pattern due to stronger winds in winter. The concentration plu-

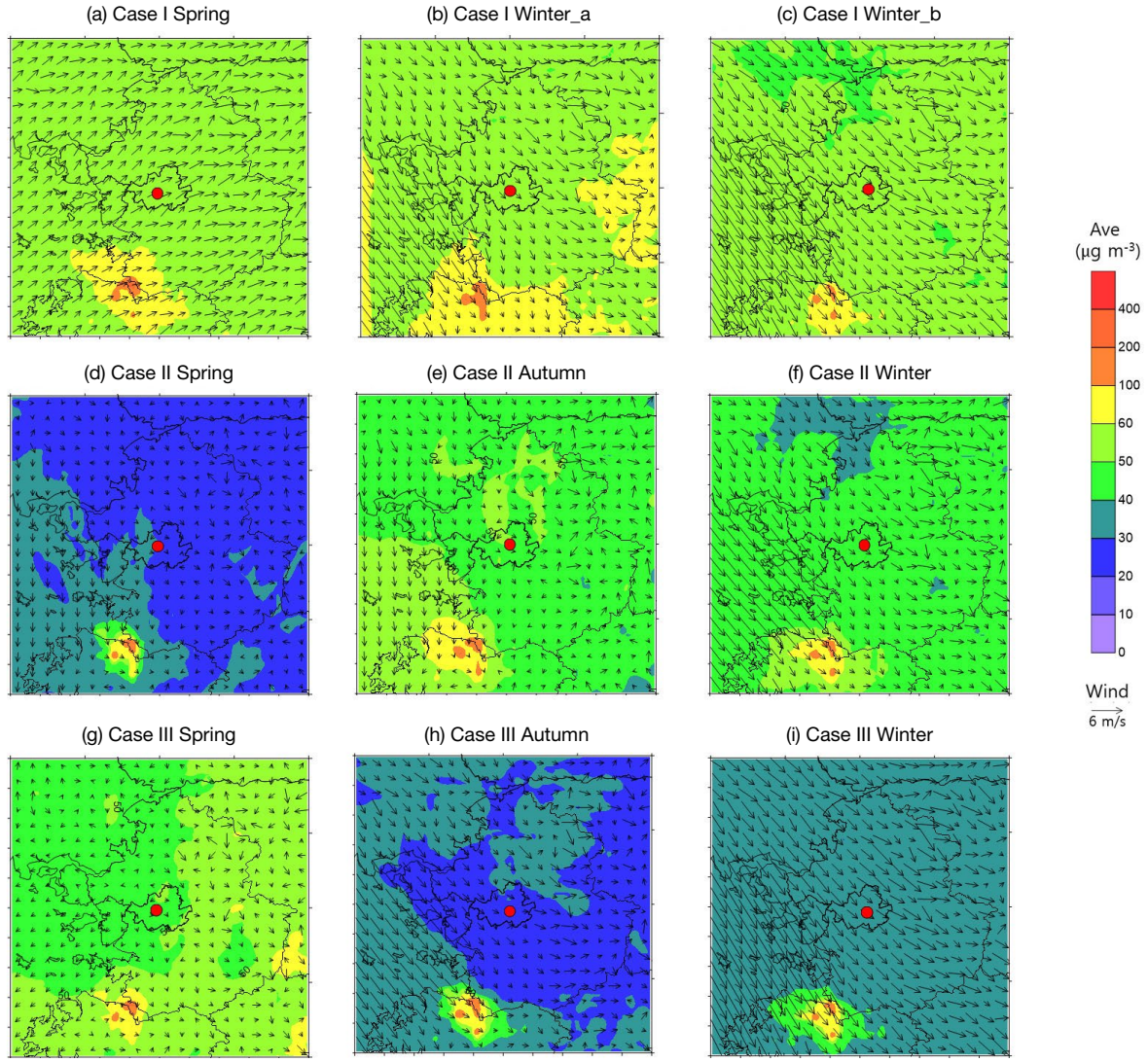

Fig. 9. The same as in Fig. 8 except for without SMA emission.

me for Case I was also broader than for Case II and Case III due to relatively strong northwesterly wind (Park *et al.*, 2004).

Fig. 9 shows the horizontal distribution of PM_{10} with the wind vector simulated without SMA emissions for the 3 cases. The overall concentration field showed a homogeneous horizontal distribution pattern except for the highest PM_{10} concentrations in the western coastal area. It should be noted that point sources including industrial combustion, electric utility, incineration, cement manufacturing, and residential heating facilities in the satellite cities located to the northeast of the SMA were important local sources that can account for at least 10 μg m^{-3} in the SMA for Case II in spring and Case III in autumn. The temporal variation of simulated PM_{10} with nationwide emissions showed higher diurnal variation and higher concentrations compared to simulated concentration without SMA emissions. $PM_{2.5}$ concentration showed less diurnal variation and lower concentrations compared to PM_{10} concentration.

5.4 Assessment of Local Emissions during High PM_{10} Concentration

The simulated average surface concentrations were used to assess the fractional contribution of total local emissions of PM_{10}, $PM_{2.5}$, NO_2, and SO_2 in the SMA during high PM concentration for each case. The contribution of local emission was assessed by analyzing the

Table 8. Fractional contribution of local emissions on the average concentrations in the SMA for the 3 cases (value considering two power plants shown in parenthesis).

Case	Season		PM_{10} ($\mu g\ m^{-3}$)	$PM_{2.5}$ ($\mu g\ m^{-3}$)	NO_2 (ppb)	SO_2 (ppb)
Case I	Spring	Nationwide	76.6	45.3	60.5	10.1
		SMA	54.9 (54.8)	29.6 (29.5)	15.7 (14.3)	4.9 (3.8)
		Reduced Conc.	21.7	15.7	44.8	5.2
		Fraction (%)	28.3 (28.5)	34.7 (34.9)	74.0 (76.4)	51.5 (62.3)
	Winter_a	Nationwide	69.3	54.6	40.8	6.2
		SMA	58.1 (58.0)	46.2 (46.2)	27.8 (27.3)	3.6 (3.3)
		Reduced Conc.	11.2	8.4	13.0	2.6
		Fraction (%)	16.1 (16.3)	15.4 (15.4)	31.9 (33.1)	41.9 (46.8)
	Winter_b	Nationwide	59.7	46.1	33.5	4.0
		SMA	54.9 (54.9)	42.6 (42.6)	24.1 (24.0)	2.7 (2.6)
		Reduced Conc.	4.8	3.5	9.4	1.3
		Fraction (%)	8.0 (8.0)	7.6 (7.6)	28.1 (28.4)	32.5 (35.0)
Case II	Spring	Nationwide	47.8	37.1	45.7	7.4
		SMA	30.3 (30.3)	24.5 (24.5)	19.7 (18.5)	3.0 (2.3)
		Reduced Conc.	17.5	12.6	26.0	4.4
		Fraction (%)	36.6 (36.6)	34.0 (34.0)	56.9 (59.5)	59.5 (68.9)
	Autumn	Nationwide	68.9	43.1	44.1	7.6
		SMA	49.4 (49.4)	29.0 (29.0)	25.1 (24.8)	3.3 (3.1)
		Reduced Conc.	19.5	14.1	21.0	4.3
		Fraction (%)	28.3 (28.3)	32.7 (32.7)	45.6 (46.2)	56.6 (59.2)
	Winter	Nationwide	59.7	44.4	43.2	6.3
		SMA	46.2 (46.2)	34.4 (34.4)	28.3 (27.8)	2.9 (2.7)
		Reduced Conc.	13.5	10.6	14.9	3.4
		Fraction (%)	22.6 (22.6)	22.5 (22.5)	34.5 (35.6)	54.0 (57.1)
Case III	Spring	Nationwide	66.2	56.4	58.4	8.4
		SMA	48.3 (48.2)	43.0 (42.9)	20.9 (20.1)	3.2 (2.5)
		Reduced Conc.	17.9	13.4	37.9	5.2
		Fraction (%)	27.0 (27.2)	23.8 (23.9)	64.5 (65.8)	61.9 (70.2)
	Autumn	Nationwide	40.0	32.0	39.6	4.3
		SMA	29.6 (29.6)	24.4 (24.4)	18.4 (18.4)	1.6 (1.6)
		Reduced Conc.	10.4	7.6	21.2	2.7
		Fraction (%)	26.0 (26.0)	23.8 (23.8)	53.5 (53.5)	62.8 (62.8)
	Winter	Nationwide	44.1	32.5	35.9	6.6
		SMA	32.8 (32.8)	24.1 (24.0)	22.0 (21.6)	3.7 (3.5)
		Reduced Conc.	11.3	8.4	13.9	2.9
		Fraction (%)	25.6 (25.6)	25.8 (26.2)	38.7 (39.8)	43.9 (47.0)

difference between model results with and without SMA emission based on nationwide emissions. This approach is basically the Brute-Force Method (BFM) by zeroing-out the emission on the targeted area (Koo *et al.*, 2009).

For Case I, the fractional contribution to the average surface concentration ranged from 8 to 28% for PM_{10}, 8 to 35% for $PM_{2.5}$, 28 to 74% for NO_2, and 33 to 52% for SO_2. For Case II, the fractional contribution to the average surface concentration ranged from 23 to 37% for PM_{10}, 23 to 34% for $PM_{2.5}$, 35 to 57% for NO_2, and 54 to 60% for SO_2. For Case III, the fractional contribution to the average surface concentration ranged from 25 to 27% for PM_{10}, 24 to 26% for $PM_{2.5}$, 39 to 65% for NO_2, and 44 to 63% for SO_2 (Table 8). Distinct characteristics for each case appeared only for Case I in winter with the fractional contribution to average surface concentration of local emissions of 8 % for PM_{10}, 8% for $PM_{2.5}$, 28% for NO_2, and 33% for SO_2.

The fractional contribution of non-SMA emissions to the SMA on the average pollutant concentration for the 3 cases was analyzed. For Case I, the fraction of non-SMA emissions was 83% for PM_{10}, 81% for $PM_{2.5}$, 55% for NO_2, and 58% for SO_2 on average. For Case II, the fraction of non-SMA emissions was 71% for PM_{10}, 70%

Table 9. Fractional contribution of non-SMA emissions on average concentrations in the SMA for the 3 cases (value considering two power plants shown in parenthesis). (unit: %)

Case	Season	PM_{10}	$PM_{2.5}$	NO_2	SO_2
Case I	Spring	72 (72)	65 (65)	26 (24)	49 (38)
	Winter_a	84 (84)	85 (85)	68 (67)	58 (53)
	Winter_b	92 (92)	92 (92)	72 (72)	68 (65)
	Avg.	83 (83)	81 (81)	55 (54)	58 (52)
Case II	Spring	63 (63)	66 (66)	43 (41)	41 (31)
	Autumn	72 (72)	67 (67)	54 (54)	43 (41)
	Winter	77 (77)	78 (78)	66 (64)	46 (43)
	Avg.	71 (71)	70 (70)	54 (53)	43 (38)
Case III	Spring	73 (73)	76 (76)	36 (34)	38 (30)
	Autumn	74 (74)	76 (76)	47 (47)	37 (37)
	Winter	74 (74)	74 (74)	61 (60)	56 (53)
	Avg.	74 (74)	75 (75)	48 (47)	44 (40)

for $PM_{2.5}$, 54% for NO_2, and 43% for SO_2 on average. For Case III, the fraction of non-SMA emissions was 74% for PM_{10}, 75% for $PM_{2.5}$, 48% for NO_2, and 44% for SO_2 on average (Table 9).

The fractional contribution for the average concentration in the SMA during high PM_{10} concentrations was consistent for the 3 cases except winter in Case I. It should be noted that the classification into the 3 cases in this study was based on the daily average PM_{10} and $PM_{2.5}$ concentrations, not meteorological characteristics. Before the maximum PM_{10} concentration at Seoul, the temporal variation for each case showed special features (Fig. 2). The PM concentrations in BND exhibited their peaks prior to those in SMA for Case I, while the latter exhibited their peaks prior to the former for Case III. Whereas the PM concentrations in both BND and Seoul exhibited their peaks at similar time for Case II.

Especially for Case II, polluted air masses from the outside of SMA were transported into the SMA by westerly (in spring) and northerly (in autumn and winter) winds before the high PM_{10} concentration events (Fig. 5). During the high PM concentration event periods in spring and autumn, stagnant synoptic systems over the Korea Peninsula, due to the surrounding pressure patterns (e.g., the high pressure system over Japan), hindered the horizontal transport and vertical dispersion of pollutants. Thus, air pollutants were accumulated, and their concentrations increased in the SMA. During the events in winter, a small-scale high pressure system was located over the Korean Peninsula. Easterly winds were too weak to disperse air pollutants effectively (Figs. 4-6).

Although the TAPM experiments indicated larger impacts of non-SMA emission and long-range transport processes on the high PM concentrations in the SMA (e.g., 71% for PM_{10}, 70% for $PM_{2.5}$, and 54% for NO_2) (Table 9), this does not mean that the contribution of local emissions was negligible, because local emissions still contributed between 30% and 50% to the high concentrations of air pollutants. This suggests that both long-range transport processes and locally emitted pollutants play a role as a contributor to high PM_{10} concentration events in the SMA.

The Dangjin and Taean power plants located on the coast southwest of the SMA have been identified as large point sources in South Korea (Park *et al.*, 2018). To assess the contribution of these two power plants to the SMA, the results for simulated average surface concentrations from emissions without emissions from the SMA and the two power plants in nationwide emissions were used. For all Cases, the fractional contributions to the SMA were negligible for PM_{10} and $PM_{2.5}$, and about 1% for NO_2 (Table 9). But, the fractional contributions for SO_2 were 6%, 5%, and 4% for Case I, Case II, and Case III, respectively. The contribution of power plant emissions to the SMA for PM_{10} and $PM_{2.5}$ in this study can be neglected. This shows that the SMA is located at an upwind location from the large two power plants during the high PM_{10} concentrations. But PM_{10} and $PM_{2.5}$ concentrations at downwind locations about 30 km distance from the power plant were reduced by 6% and 4%, respectively, similar to the estimate in previous studies (Park *et al.*, 2018). This implies that local emissions from line sources in the SMA are a major source of PM_{10}.

6. CONCLUSIONS

The results of this study have shown that Case I in winter was influenced by long range transboundary processes. The PM_{10} and $PM_{2.5}$ concentrations in the SMA showed a lag time 6 to12 h for the maximum concentration compared to BND. Case III was influenced by the accumulation of local and neighboring (non-SMA) emissions by atmospheric stagnation. After the PM_{10} and $PM_{2.5}$ concentrations in the SMA increased, concentrations in BND sharply decreased. Case II was a mixed case between Case I and Case III with local circulation. The PM_{10} and $PM_{2.5}$ concentrations in the SMA were nearly the same as concentrations in BND. The maxi-

mum PM concentrations in BND occurred 6 h later than in the SMA by air parcels advected from the SMA.

Our study shows that the high PM_{10} concentrations in the SMA were mostly governed by the conditions for Case II (45 among total 65 occurrence days) compared to for Case I (12 days) and Case III (8 days) and that nearly 50% occurred in spring (total 32 for Case I, 26 for Case II and 2 for Case III). Prior to the PM_{10} concentration reaching the peak concentration, the pattern in each case was distinct. After that, the pattern for the 3 cases became less distinct, and the meteorological conditions were characterized by local circulation systems with weak wind, particularly in spring. The classification into the 3 cases in this study was based on the daily average PM_{10} and $PM_{2.5}$ concentrations, not meteorological characteristics. Therefore, the fractional contribution to the average concentration in the SMA during the high PM_{10} concentration, except for winter_b for Case I dominated by the Siberian high pressure system, was consistent among the 3 cases. This implies that the local and neighboring (non-SMA) emissions during high PM_{10} concentration in the SMA particularly in spring were the major sources rather than emissions from long-range transboundary processes and most of the non-SMA contribution to PM_{10} and $PM_{2.5}$ resulted from neighboring emissions. Particularly, approximately 1600 stacks from combustion sources in the SMA and mostly industrial sources including electric industrial combustion, electric utility, incineration, cement manufacturing, and residential heating in the satellite cities located to the southeast and east of the SMA were important sources of local emissions in addition to mobile sources. The fractional contributions to high PM_{10}, and $PM_{2.5}$ in the SMA at upwind location from two large power plants were negligible compared to about 6% and 4% contributions to PM_{10}, and $PM_{2.5}$ in the other areas at downwind locations.

High PM_{10} concentrations in the SMA in winter mainly resulted from long-range transboundary processes by the Siberian high pressure system. It will be valuable to confirm the fractional contribution to the SMA from long-range transboundary processes in future studies using other research approaches.

ACKNOWLEDGEMENT

This work was funded by the Korea Meteorological Administration Research and Development Program under Grant KMI2018-05310. All meteorological data used in this study were jointly provided by the Korea Meteorological Administration (Weather Information Service Engine Project), Hankuk University of Foreign Studies, and National Institute of Meteorological Sciences. We also thank National Institute of Environmental Research for providing Korean emission data from the Clean Air Policy Support System (CAPSS). We would like to acknowledge Jung-Hun Woo at Konkuk University for providing the aggregated Korean emission data by major sectors.

REFERENCES

Azzi, M., Johnson, G.M., Cope, M. (1992) An introduction to the generic reaction set photochemical smog mechanism. Proceedings of the 11th International Clean Air and Environment Conference, Brisbane, Clean Air Society of Australia & New Zealand.

Barmpadimos, I., Hueglin, C., Keller, J., Henne, S., Prevot, A.S.H. (2011) Influence of meteorology on PM_{10} trends and variability in Switzerland from 1991 to 2008. Atmospheric Chemistry and Physics 11, 1813–1835, DOI: 10.5194/acp-11-1813-2011.

Demographia (2018) Demographia world urban areas, built up urban areas or world agglomerations, 14th edit, Demographia, Illinois, USA, 118pp. http://demographia.com/db-worldua.pdf.

Hurley, P.J. (2008) TAPM V4. Part 1: Technical Description, CSIRO Marine and Atmospheric Research Paper No. 25, 59pp.

Hurley, P.J., Mary, E., Ashok, L. (2008) TAPM V4. Part 2: Summary of Some Verification Studies. CSIRO Marine and Atmospheric Research Paper No. 26, 31pp.

Jo, H.-Y., Kim, C.-H. (2013) Identification of long-range transported haze phenomena and their meteorological features over Northeast Asia. Journal of Applied Meteorology and Climatology 52, 1318–1328, DOI: 10.1175/JAMC-D-11-0235.1.

Kim, C.-H., Park, S.-Y., Kim, Y.-J., Chang, L.-S., Song, S.-K., Moon, Y.-S., Song, C.-K. (2012) A numerical study on indicators of long-range transport potential for anthropogenic particulate matters over northeast Asia. Atmospheric Environment 58, 35–44, DOI: 10.1016/j.atmosenv.2011.11.002.

Kim, H.C., Kim, E., Bae, C., Cho, J.H., Kim, B.U., Kim, S. (2017) Regional contributions to particulate matter contribution in the Seoul Metropolitan Area, Korea: Seasonal variation and sensitivity to meteorology and emission inventory. Atmospheric Chemistry and Physics 17, 10315–10332, DOI: 10.5194/acp-17-10315-2017.

KMOE (The Ministry of Environment in Korea) (2017) Press report (July 26): Reduction effect of shut down of old power plants during June 2017, Sejong-si, South Korea.

Koo, B., Wilson, G.M., Morris, R.E., Dunker, A.M., Yarwood,

G. (2009) Comparison of source apportionment and sensitivity analysis in a particulate matter air quality model. Environmental Science and Technology 43(17), 6669–6675.

Kwon, T.H., Park, M.-S., Yi, C., Choi, Y.J. (2014) Effects of different averaging operators on the urban turbulent fluxes. Atmosphere Korean Meteorological Society 24, 197–206, DOI: 10.14191/Atmos.2014.24.2.197.

Li, X., Wang, Y., Zhao, H., Hong, Y., Liu, N., Ma, J. (2018) Characteristics of pollutants and boundary layer structure during two haze events in summer and autumn 2014 in Shenyang, Northeast China. Aerosol and Air Quality Research 18, 386–396, DOI: 10.4209/aaqr.2017.03.0100.

NIER (National Institute of Environmental Research in Korea) (2017) Introduction to the KORUS-AQ Rapid Science Synthesis Report, Incheon, South Korea, 24 pp.

Park, I.-S. (2014) Creative counter-measures of PM_{10}. Journal of Korean Society for Atmospheric Environment 30(2), 211–212.

Park, I.-S. (2016) Why do the high concentration PM_{10} episodes occur and what is the major cause of the episodes? Journal of Korean Society for Atmospheric Environment 32(3), 352–353.

Park, I.-S., Choi, W.-J., Lee, T.-Y., Lee, S.-J., Han, J.-S., Kim, C.-H. (2005) Simulation of long-range transport of air pollutants over Northeast Asia using a comprehensive acid deposition model. Atmospheric Environment 39, 4075–4085, DOI: 10.1016/j.atmosenv.2005.03.038.

Park, I.-S., Lee, S.-J., Kim, C.-H., Yoo, C., Lee, Y.-H. (2004) Simulating urban-scale air pollutants and their predicting capabilities over the Seoul Metropolitan Area. Journal of the Air & Waste Management Association 54, 695–710.

Park, I.-S., Song, C.-K., Park, M.-S., Kim, B.-G., Jang, Y.-W., Ha, S.-S., Jang, S.-H., Chung, K.-W., Lee, H.-J., Lee, U.-J., Kim, S.-K., Kim, C.-H. (2018) Numerical study on the impact of power plants on primary PM_{10} concentrations in South Korea. Asian Journal for Atmospheric Environment 12(3), 255–273, DOI: 10.5572/ajae.2018.12.3.255.

Park, M.-S. (2018) Overview of meteorological surface variables and boundary-layer Structures in the Seoul Metropolitan Area during the MAPS-Seoul Campaign. Aerosol and Air Quality Research 18, 2157-2172. DOI: 10.4209/aaqr.2017.10.0428.

Park, M.-S., Chae, J.-H. (2018) Features of sea-land-breeze circulation over the Seoul Metropolitan Area. Geoscience Letters 5, 28, DOI: 10.1186/s40562-018-0127-6.

Park, M.-S., Joo, S.J., Park, S.-U. (2014) Carbon dioxide concentration and flux in an urban residential area in Seoul, Korea. Advances in Atmospheric Sciences 31, 1101–1112, DOI: 10.1007/s00376-013-3168-y.

Park, M.-S., Park, S.-H., Chae, J.-H., Choi, M.-H., Song, Y., Kang, M., Rho, J.-W. (2017) High-resolution urban observation network for user-specific meteorological information service in the Seoul Metropolitan Area, South Korea. Atmospheric Measurement Techniques 10, 1575–1594, DOI: 10.5194/amt-10-1575-2017.

Park, S.-U., Lee, I.H., Choe, A., Joo, S.J. (2015) Contributions of the pollutant emission in South Korea to the aerosol concentrations and depositions in Asia. Asia-Pacific Journal of Atmospheric Sciences 51, 183–195, DOI: 10.1007/s13143-015-0069-2.

Seo, J., Kim, J.Y., Yoon, D., Lee, J.Y., Kim, H., Lim, Y.B., Kim, Y., Jin, H.C. (2017) On the multiday haze in the Asian continental outflow: the important role of synoptic conditions combined with regional and local sources. Atmospheric Chemistry and Physics 17, 9311–9332, DOI: 10.5194/acp-17-9311-2017.

Seo, J., Park, D.-S. R., Kim, J.Y., Youn, D., Lim, Y.B., Kim, Y. (2018) Effects of meteorology and emissions on urban air quality: a quantitative statistical approach to long-term records (1999–2016) in Seoul, South Korea. Atmospheric Chemistry and Physics 18, 16121–16137, 2018, DOI: 10.5194/acp-8-16121-2018.

Venkatram, A., Karamchandani, P., Pai, P., Sloane, C., Saxena, P., Goldstein, R. (1997) The development of a model to examine source-receptor relationships for visibility on the Colorado Plateau. Journal of the Air and Waste Management Association 47, 286-301, DOI: 10.1080/10473289.1997.1046453.

Wang, S., Zhou, P., Lin, L., Liu, C., Huang, T. (2018) Influence of major urban construction on atmospheric particulates and emission reduction measures. Asian Journal for Atmospheric Environment 12(3), 215-231, DOI: 10.5572/ajae.2018.12.3.215.